Available online at www.sciencedirect.com
SCIENCE DIRECT®
International Journal of Thermal Sciences 42 (2003) 713–723
International Journal of Thermal Sciences
www.elsevier.com/locate/ijts

Performance evaluation of branching and impacting tee junctions for laminar forced-convection applications

A.M.F. El-Shaboury, H.M. Soliman *, S.J. Ormiston

Department of Mechanical and Industrial Engineering, University of Manitoba, Winnipeg, MB, Canada R3T 5V6

Received 15 April 2002; accepted 3 October 2002

Abstract

The governing equations for mass, momentum, and energy conservation have been solved numerically for laminar forced convection in two-dimensional branching and impacting tee junctions. The resulting velocity, temperature, and pressure fields were used in computing important engineering parameters, such as the wall shear stress, wall heat flux, pumping power, and excess heat transfer. These parameters are presented for the two junctions in a comparative fashion over a wide range of mass splits and two values of the inlet Reynolds number. It is shown that the two junctions may have similar distributions of wall shear stress and wall heat flux at certain flow splits. Results of the performance evaluation can guide the designer in selecting the appropriate configuration (branching or impacting) based on the pumping power requirement, excess heat transfer, or excess heat transfer per unit pumping power.

Keywords: Tee junctions; Branching and impacting; Numerical analysis; Pumping power; Heat transfer

1. Introduction

Fluid flow in 90° tee junctions is of considerable importance in many engineering and biomedical applications. The most commonly used flow configurations are the branching and the impacting tees. Two important parameters can be used in deciding which flow configuration is desirable for a particular application. The first parameter is the pumping power required to push the flow through the junction, and the second one is the excess heat transfer resulting from the flow split in the junction.

The basic characteristics of laminar forced convection in two-dimensional tee junctions were investigated for the branching flow configuration (e.g., [1–4]) and the impacting flow configuration (e.g., [5–7]). These studies produced separate results for each configuration that included wall-shear-stress distribution, velocity profiles, streamlines, pressure loss coefficients, wall-heat-flux distributions, isotherms, and overall rate of heat transfer. However, there have been no comparative studies between the two sets of results or data on the pumping power and excess heat transfer that can be used in design.

The main objective of this paper is to conduct a performance evaluation of the pressure drop and heat transfer characteristics of two-dimensional branching and impacting tees. These results would help the designer decide which flow configuration is more desirable in terms of pumping power and heat transfer. Also, this study investigates the flow conditions under which the fluid flow and heat transfer characteristics are similar for both configurations.

2. Mathematical formulation

2.1. Geometry and flow conditions

The geometry of the two tee junctions considered in this investigation is shown in Fig. 1. Fully developed flow (hydrodynamically and thermally) enters the duct through the inlet region with a mass flow rate $\dot{m}'_{\text{in}}$ (per unit depth) and a bulk temperature T_{in}. At the junction region, the flow splits such that the ratio of outlet-3 mass flow rate to the inlet mass flow rate is β. The inlet, outlet-2, and outlet-3 have lengths L_1, L_2, and L_3, respectively, and the channel

* Corresponding author.
E-mail address: hsolima@cc.umanitoba.ca (H.M. Soliman).

1290-0729/03/$ – see front matter
doi:10.1016/S1290-0729(03)00039-5

Nomenclature

c_p	specific heat	$J\cdot kg^{-1}\cdot K^{-1}$
E	pumping power	$W\cdot m^{-1}$
H	duct size in the inlet, outlet-2, and outlet-3	m
k	thermal conductivity	$W\cdot m^{-1}\cdot K^{-1}$
L	duct length	m
$\dot{m}'$	mass flow rate per unit depth	$kg\cdot m^{-1}\cdot s^{-1}$
p	pressure	Pa
Pr	Prandtl number	
Q	total rate of heat transfer per unit depth	$W\cdot m^{-1}$
q	local heat flux	$W\cdot m^{-2}$
Re	Reynolds number	
T	temperature	K
u	velocity component in the x direction	$m\cdot s^{-1}$
V	cross-sectional average velocity	$m\cdot s^{-1}$
v	velocity component in the y direction	$m\cdot s^{-1}$
x, y	Cartesian co-ordinates	m

Greek symbols

β	ratio of outlet-3-to-inlet mass flow rates	
ν	kinematic viscosity	$m^2\cdot s^{-1}$
ρ	density	$kg\cdot m^{-3}$
τ	shear stress	Pa

Subscripts

1, 2, 3	inlet, outlet-2, and outlet-3
21	heat-transfer portion of outlet-2
22	adiabatic portion of outlet-2
31	heat-transfer portion of outlet-3
32	adiabatic portion of outlet-3
in	inlet face
w	at the wall

Superscript

$*$	dimensionless quantity

height in all three sides of the junction is H. The inlet length L_1 was set to a value of 20 H in order to ensure that the inlet flow remains fully developed over a significant length before the junction effects begin. Also, L_2 and L_3 were set to a value of 100 H in order to ensure that the flows in outlet-2 and outlet-3 achieve fully developed conditions over a considerable length before leaving the duct.

Heat transfer takes place between the walls and the fluid throughout the inlet region, a portion of outlet-2 with length L_{21}, and a portion of outlet-3 with length L_{31}. The remaining portions of the walls in outlet-2 and outlet-3 are adiabatic. All walls in the heat-transfer section of the junction are kept at a uniform temperature T_w. The heated sections of outlet-2 and outlet-3 were selected as $L_{21}/H = L_{31}/H = 30$. These lengths were found to be sufficient (under all flow conditions considered) to achieve (or approach) thermally-fully-developed flow at the end of the heat-transfer sections in outlet-2 and outlet-3.

2.2. Governing equations

The flow is considered to be two-dimensional, steady, and laminar. The fluid is incompressible and Newtonian, and the properties are assumed to be constant. Body forces and viscous dissipation are assumed to be negligible. Under these conditions, the governing continuity, momentum, and energy equations can be expressed in the following non-dimensional form:

$$\frac{\partial u^*}{\partial x^*} + \frac{\partial v^*}{\partial y^*} = 0 \tag{1}$$

$$u^*\frac{\partial u^*}{\partial x^*} + v^*\frac{\partial u^*}{\partial y^*} = -\frac{1}{2}\frac{\partial p^*}{\partial x^*} + \left(\frac{2}{Re_1}\right)\left(\frac{\partial^2 u^*}{\partial x^{*2}} + \frac{\partial^2 u^*}{\partial y^{*2}}\right) \tag{2}$$

$$u^*\frac{\partial v^*}{\partial x^*} + v^*\frac{\partial v^*}{\partial y^*} = -\frac{1}{2}\frac{\partial p^*}{\partial y^*} + \left(\frac{2}{Re_1}\right)\left(\frac{\partial^2 v^*}{\partial x^{*2}} + \frac{\partial^2 v^*}{\partial y^{*2}}\right) \tag{3}$$

$$u^*\frac{\partial T^*}{\partial x^*} + v^*\frac{\partial T^*}{\partial y^*} = \left(\frac{2}{Re_1 Pr}\right)\left(\frac{\partial^2 T^*}{\partial x^{*2}} + \frac{\partial^2 T^*}{\partial y^{*2}}\right) \tag{4}$$

where the non-dimensional parameters are defined by

$$x^* = \frac{x}{H}, \qquad y^* = \frac{y}{H}, \qquad L^* = \frac{L}{H} \tag{5a}$$

$$u^* = \frac{u}{V_1}, \qquad v^* = \frac{v}{V_1}$$

$$p^* = \frac{p}{(\rho V_1^2)/2}, \qquad T^* = \frac{T - T_{in}}{T_w - T_{in}} \tag{5b}$$

$$Re_1 = \frac{2HV_1}{\nu}, \qquad Pr = \frac{\rho\nu c_p}{k} \tag{5c}$$

and V_1 is the mean inlet velocity given by

$$V_1 = \frac{\dot{m}'_{in}}{\rho H} \tag{5d}$$

2.3. Boundary conditions

The applicable boundary conditions are as follows:

(1) *Inlet face*: At $x^* = -(L_1^* + 0.5)$ and $-0.5 \leqslant y^* \leqslant 0.5$, $u^* = 1.5(1 - 4y^{*2})$, $v^* = 0$, and a fully developed temperature profile corresponding to a dimensionless bulk temperature $T_{in}^* = 0$ were imposed.
(2) *Walls*: $u^* = v^* = 0$ on all walls, $T^* = 1$ on the heated walls, and $\partial T^*/\partial n^* = 0$ on the adiabatic walls, where n is the direction normal to the walls.

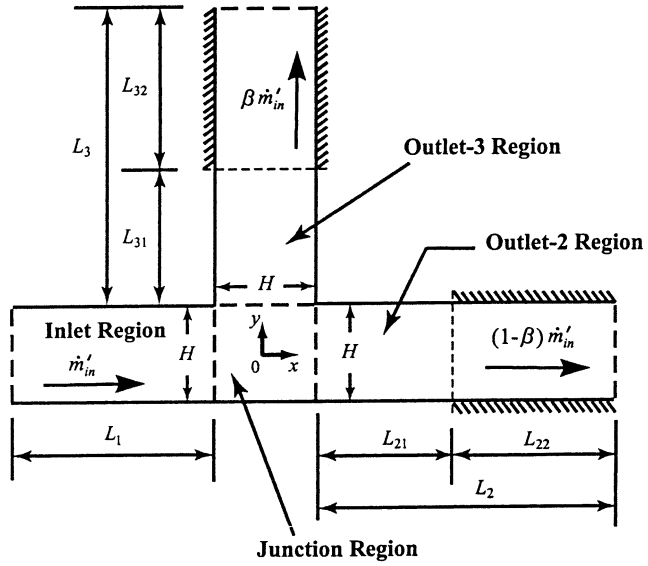

(a) Branching

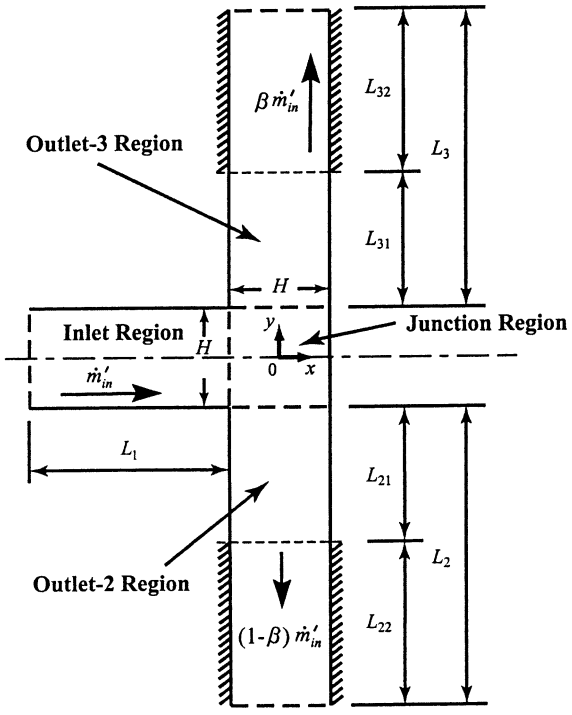

(b) Impacting

Fig. 1. Geometry and co-ordinate system.

(3) *Outlet-2 face*: A reference pressure, $p = 0$ (or $p^* = 0$), was specified at a single node on the outlet face, and $\partial T^*/\partial n^* = 0$ was specified at all nodes, where n is the direction normal to the face.
(4) *Outlet-3 face*: At $-0.5 \leqslant x^* \leqslant 0.5$ and $y^* = (L_3^* + 0.5)$, a total mass flow rate of $\beta \dot{m}'_{\text{in}}$ was specified, and $\partial T^*/\partial y^* = 0$ was imposed.

The mathematical formulation of the problem consisting of the governing equations and boundary conditions suggests that the velocity, pressure, and temperature fields (u^*, v^*, p^*, T^*) at any point (x^*, y^*) within the flow domain are functions of the following set of independent parameters:

- The geometry parameters L_1^*, L_2^*, L_3^*, L_{21}^*, and L_{31}^*.
- The flow parameters Re_1 and β.
- The property parameter Pr.

All the present results correspond to $L_1^* = 20$, $L_2^* = L_3^* = 100$, $L_{21}^* = L_{31}^* = 30$, and $Pr = 0.7$. Therefore, the only remaining independent parameters are Re_1 and β.

The velocity and temperature fields were used in calculating some parameters of engineering importance. These are the local (dimensionless) wall shear stress τ_{w}^* and the local (dimensionless) wall heat flux q_{w}^*. The parameter τ_{w}^* is defined as

$$\tau_{\text{w}}^* = \frac{\tau_{\text{w}}}{(\rho V_1^2)/2} \tag{6}$$

where τ_{w} is the local wall shear stress. In dimensionless form,

$$\tau_{\text{w}}^* = \left(\frac{4}{Re_1}\right)\frac{\partial u^*}{\partial n^*}\bigg|_{\text{wall}} \tag{7}$$

where n^* is the dimensionless coordinate normal to the wall. The local wall heat flux is given by

$$q_{\text{w}}^* = \frac{q_{\text{w}}}{k(T_{\text{w}} - T_{\text{in}})/(2H)} \tag{8}$$

where q_{w} is the local wall heat flux, $q_{\text{w}} = -k(\partial T/\partial n)_{\text{w}}$.

3. Numerical solution

The numerical solution of the governing equations was obtained using CFX-TASCflow, version 2.10. This code uses a finite volume method [8] but is based on a finite element approach of representing the geometry. Mass conservation discretization was applied on a non-staggered grid. The discretized mass, momentum, and energy equations were solved iteratively using an additive correction multi-grid method to accelerate convergence. The solution was considered converged when the sum of residuals was less than 1×10^{-5}. More details can be found in [4,7].

3.1. Computational mesh

Four different grid blocks were created for the inlet, junction, outlet-2, and outlet-3 regions of each tee junction. The grid blocks in the outlet-2 and outlet-3 regions were each divided into two sub-blocks; the first one was for the heated section and the second was for the adiabatic section. Each sub-block had uniform grid spacing in itself; however, the two sub-blocks had different grid spacing when compared to each other. The computational grid for the

Table 1
Details of grids used in mesh-independence tests for the impacting junction

	Inlet region		Junction region		Outlet-2 region				Outlet-3 region			
					Heated section		Adiabatic section		Heated section		Adiabatic section	
	nx	*ny*	*nx*	*ny*	*nx*	*ny*	*nx*	*ny*	*nx*	*ny*	*nx*	*ny*
Grid 1	40	30	30	30	30	200	30	85	30	200	30	85
Grid 2	70	60	60	60	60	400	30	170	60	400	30	170
Grid 3	100	91	91	91	91	600	31	250	91	600	31	250
Grid 4	200	121	121	121	121	800	41	350	121	800	41	350

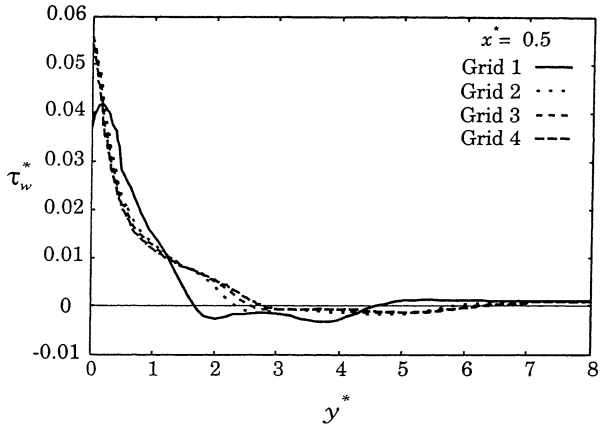

(a) Wall Shear Stress

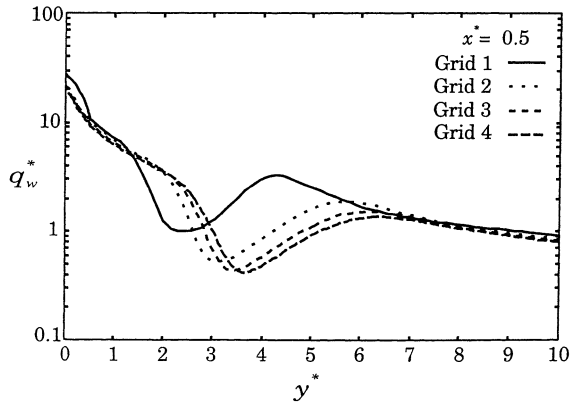

(b) Wall Heat Flux

Fig. 2. Sample of grid-independence tests (impacting junction with $\beta = 0.1$, $Pr = 0.7$ and $Re_1 = 2000$).

whole flow domain was then formed by attaching the four grid blocks together. It was decided to use the finest possible grid spacing in the junction region to account for the steep gradients in the solution field expected in this area.

Mesh-independence tests were carried out for both types of junction by varying the number of nodes in the inlet, junction, outlet-2, and outlet-3 regions, separately. Table 1 provides a detailed description of the grids used in the mesh-independence tests for the impacting junction (similar grids were used for the branching junction). The tests were carried out for two conditions: $\beta = 0.1$ and 0.9; both with $Re_1 = 2000$ and $Pr = 0.7$.

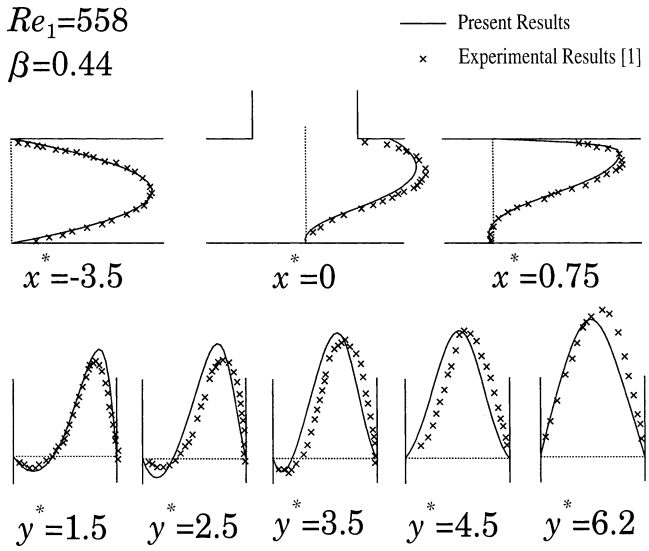

Fig. 3. Comparison with the experimental results of Liepsch et al. [1].

A representative sample of the grid-independence tests is shown in Fig. 2 corresponding to $\beta = 0.1$ in an impacting junction. The results in Fig. 2 are in terms of τ_w^* and q_w^* along $x^* = 0.5$. Fig. 2(a) shows that the values of τ_w^* from grids 3 and 4 are nearly identical. On the other hand, Fig. 2(b) shows that there is a noticeable (percentage) difference in the values of q_w^* from grids 3 and 4, mainly in the region $2 \leqslant y^* \leqslant 8$. However, it can be argued that the deviation between grids 3 and 4 is small in absolute terms. Similar results were obtained for $\beta = 0.9$.

Based on the above results and other grid-independence tests (not shown), the final mesh for the present investigation was selected to be grid 3. A typical execution time using the final mesh was about 110 CPU hours on a DEC/Compaq Alphastation 500 au.

3.2. Comparison with earlier work

Several comparisons were made with earlier work in order to validate the numerical method used in the present investigation. Two comparisons are shown here as a sample; one for the branching and the other for the impacting junction.

Fig. 3 shows a comparison between the computed velocity profiles and the experimental velocity profiles reported by Liepsch et al. [1] for a branching junction at $Re_1 = 558$ and

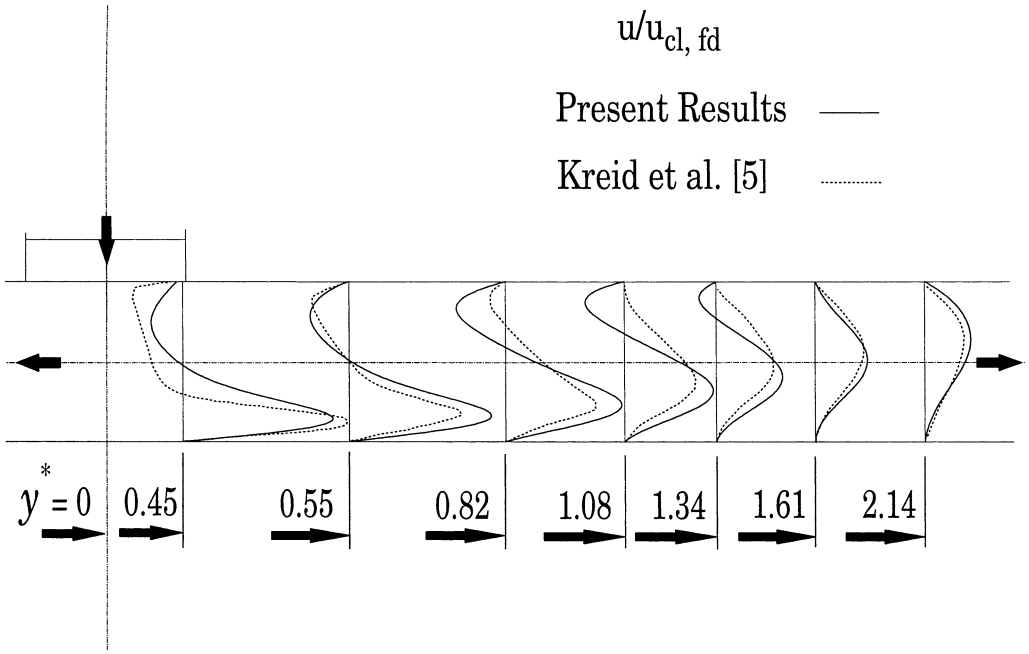

Fig. 4. Comparison with the experimental results of Kreid et al. [5].

$\beta = 0.44$. These results correspond to water flow in a junction with the following geometry: $L_1^* = 109.5$, $L_2^* = 94.5$, and $L_3^* = 81$. The agreement between the numerical and experimental results is good at the various locations shown.

Direct validation for the impacting junction was not possible due to lack of similar results. The closest match to the present conditions is the experimental measurements of the laminar velocity profiles in outlet-3 of an impacting junction constructed from tubes with circular cross-sections, reported by Kreid et al. [5]. The results in [5] correspond to water flow, an inside diameter of 9.5 mm on all sides of the junction, $V_1 = 0.0387$ m·s^{-1}, and $\beta = 0.0614$. Results were generated for the present (two-dimensional) geometry using water properties, $H = 9.5$ mm, and the same values of V_1 and β used in [5]. It is recognized that quantitative agreement between the two sets of results is not expected due to the difference in geometry. Fig. 4 shows a comparison between the present profiles of $u/u_{\mathrm{cl,fd}}$ and the measured profiles reported in [5] along outlet-3, where $u_{\mathrm{cl,fd}}$ is the fully developed value of the centreline velocity in outlet-3. There is a definite similarity in trend between the two sets of profiles. A re-circulation zone can be seen in the top part of outlet-3 in both cases. The extent of this zone in the y direction is longer for the planar junction. As well, a jetting zone exists underneath the re-circulation zone in both cases with fairly similar strength.

4. Results and discussion

Results were obtained for both flow configurations corresponding to $0.1 \leqslant \beta \leqslant 0.9$, and $Re_1 = 1000$ and 2000. The focus here will be on the similarity (or lack of it) between the two configurations and the performance evaluation of both.

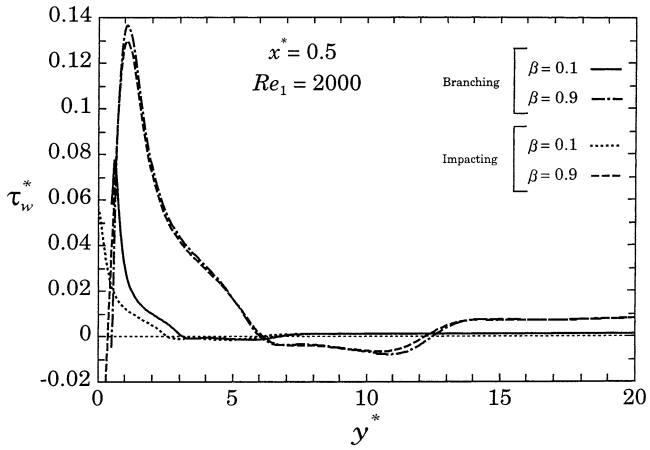

Fig. 5. Wall shear stress in outlet-3, $x^* = 0.5$.

4.1. Wall shear stress

Fig. 5 shows the variation of τ_w^* in outlet-3 of both configurations along $x^* = 0.5$ for $Re_1 = 2000$, and $\beta = 0.1$ and 0.9. It can be seen that for $\beta = 0.9$, the distribution of τ_w^* is almost identical for the two types of junctions. For $\beta = 0.1$, there is a small difference in the results in the range of $0 \leqslant y^* \leqslant 3$. Also, the size and the location of the re-circulation zones (where τ_w^* becomes negative) are almost identical for both junctions.

Fig. 6 shows the variation of τ_w^* on the other wall of outlet-3 ($x^* = -0.5$) with similar trends to those seen in Fig. 5. This similarity in τ_w^*-distribution is very interesting

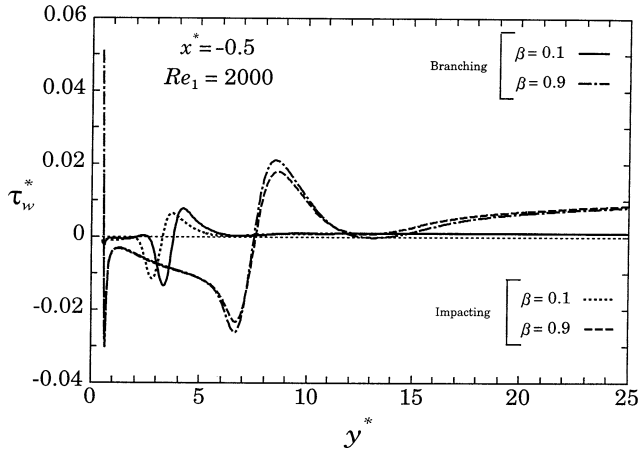

Fig. 6. Wall shear stress in outlet-3, $x^* = -0.5$.

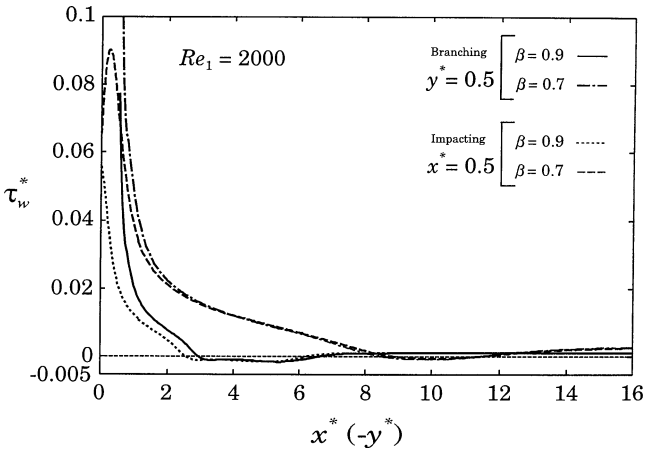

Fig. 7. Wall shear stress along one wall in outlet-2.

in view of the significantly different flow configuration between the two junctions.

For mass splits between $\beta = 0.1$ and $\beta = 0.9$, the similarity in wall shear stress illustrated in Figs. 5 and 6 disappeared and significant differences in magnitude and trend were found in τ_w^* between the two junctions.

Fig. 7 shows the variation of τ_w^* along one of the walls of outlet-2 for $Re_1 = 2000$, and $\beta = 0.7$ and 0.9. It can be seen that there is similarity in trend between the two junctions. In terms of magnitudes, there are small deviations only in the range $0 \leqslant y^* \leqslant 3$. These exact trends were also found to be valid along the other wall of outlet-2 at the same values of β.

All the observations made above for $Re_1 = 2000$ were also found to be valid for $Re_1 = 1000$.

4.2. Streamlines

Fig. 8 shows the streamlines in both configurations for the case of $Re_1 = 2000$ and $\beta = 0.9$. Surprisingly, the streamlines in both outlets are similar for the two types of the junctions. The size and the location of the four re-circulation zones formed on the walls are almost identical. The above observations are consistent with the results in Figs. 5–7, where values of τ_w^* are almost identical on all the walls of the junction for the case of $\beta = 0.9$.

Fig. 9 shows the streamlines in both configurations for the case of $Re_1 = 2000$ and $\beta = 0.1$. It can be seen that the streamlines are similar only in outlet-3, which carries 10% of the inlet mass flow rate. In the other outlet, the streamlines are completely different in shape. The above observations are consistent with the results in Figs. 5 and 6, where values of τ_w^* in outlet-3 are very similar for the case of $\beta = 0.1$. These observations are also consistent with Fig. 7, where values of τ_w^* in outlet-2 were found to be similar only for high values of β.

In order to complete the study of the effect of β on the flow structure, the streamlines for an even flow split ($\beta = 0.5$) were obtained and the results are shown in Fig. 10. It is clear from this figure that the similarity in flow structure between impacting and branching junctions disappears in both outlet-2 and outlet-3 regions at this value of β. Thus, the similarity in flow structure between the two junctions exists in both outlets for high β, outlet-3 only for low β, and disappears from both outlets at intermediate values of β.

4.3. Wall heat flux

Figs. 11 and 12 show the variation of q_w^* along both walls of outlet-3 of the two configurations for $Re_1 = 2000$, and $\beta = 0.1$ and 0.9. It is clear that for $\beta = 0.9$, the distribution of q_w^* is almost identical for the two junctions. For $\beta = 0.1$, the results have the same trend with a small difference in magnitude in the range $0 \leqslant y^* \leqslant 7$. These observations are consistent with those seen in Figs. 5, 6, and 8. This similarity in q_w^*-distribution at $\beta = 0.1$ and 0.9 was also found to be valid at $Re_1 = 1000$. However, for values of β between 0.1 and 0.9, this similarity was found to disappear, as was the case for τ_w^*.

Fig. 13 shows the variation of q_w^* along one of the walls of outlet-2 for $Re_1 = 2000$, and $\beta = 0.7$ and 0.9. It can be seen that there is similarity in trend between the two junctions. In terms of magnitudes, there are small deviations only in the range $0 \leqslant y^* \leqslant 3$. These exact trends were also found to be valid along the other wall of outlet-2 at the same values of β. All these results are consistent with those seen earlier in Figs. 7 and 8.

All the observations made above for $Re_1 = 2000$ were also found to be valid for $Re_1 = 1000$.

4.4. Pumping power

The pumping power E is defined as the rate of mechanical energy loss due to mass split at the junction. The value of E can be determined by applying an energy balance on a control volume surrounding the junction region (excluding the three arms of the junction). Accordingly, for both flow configurations, the value of E is given by,

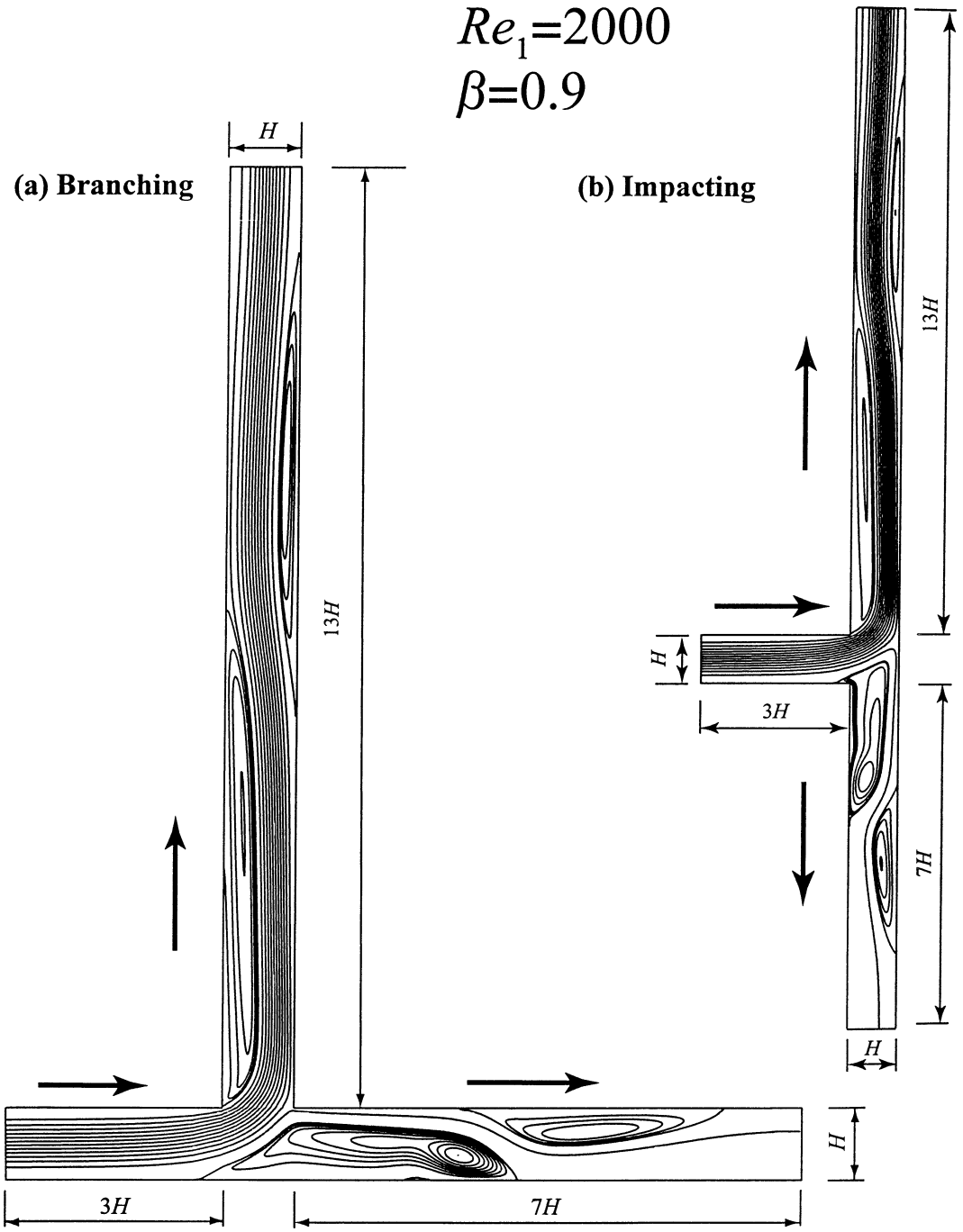

Fig. 8. Streamlines for $Re_1 = 2000$ and $\beta = 0.9$.

$$E = \dot{m}'_{\text{in}}\left[\frac{p_{\text{m1}}}{\rho} + \frac{V_1^2}{2}\right] - \dot{m}'_{\text{in}}(1-\beta)\left[\frac{p_{\text{m2}}}{\rho} + \frac{V_2^2}{2}\right] - \dot{m}'_{\text{in}}\beta\left[\frac{p_{\text{m3}}}{\rho} + \frac{V_3^2}{2}\right] \tag{9}$$

where p_{m1}, p_{m2}, and p_{m3} are the mean pressures at sides 1, 2, and 3 of the junction extrapolated from the fully developed regions of the inlet, outlet-2, and outlet-3 regions. In dimensionless form,

$$E^* = (1-\beta)\left[\left(p^*_{\text{m1}} - p^*_{\text{m2}}\right) + \beta(2-\beta)\right] + \beta\left[\left(p^*_{\text{m1}} - p^*_{\text{m3}}\right) + 1 - \beta^2\right] \tag{10}$$

where $E^* = E/(\dot{m}'_{\text{in}} V_1^2/2)$.

Fig. 14 shows the variation of E^* with β for $Re_1 = 1000$ and 2000. Fig. 14 shows that Re_1 has insignificant effect on E^*. As well, for the impacting junction, values of E^* are symmetric around $\beta = 0.5$ with E^* reaching a minimum value at this condition. This symmetry in the

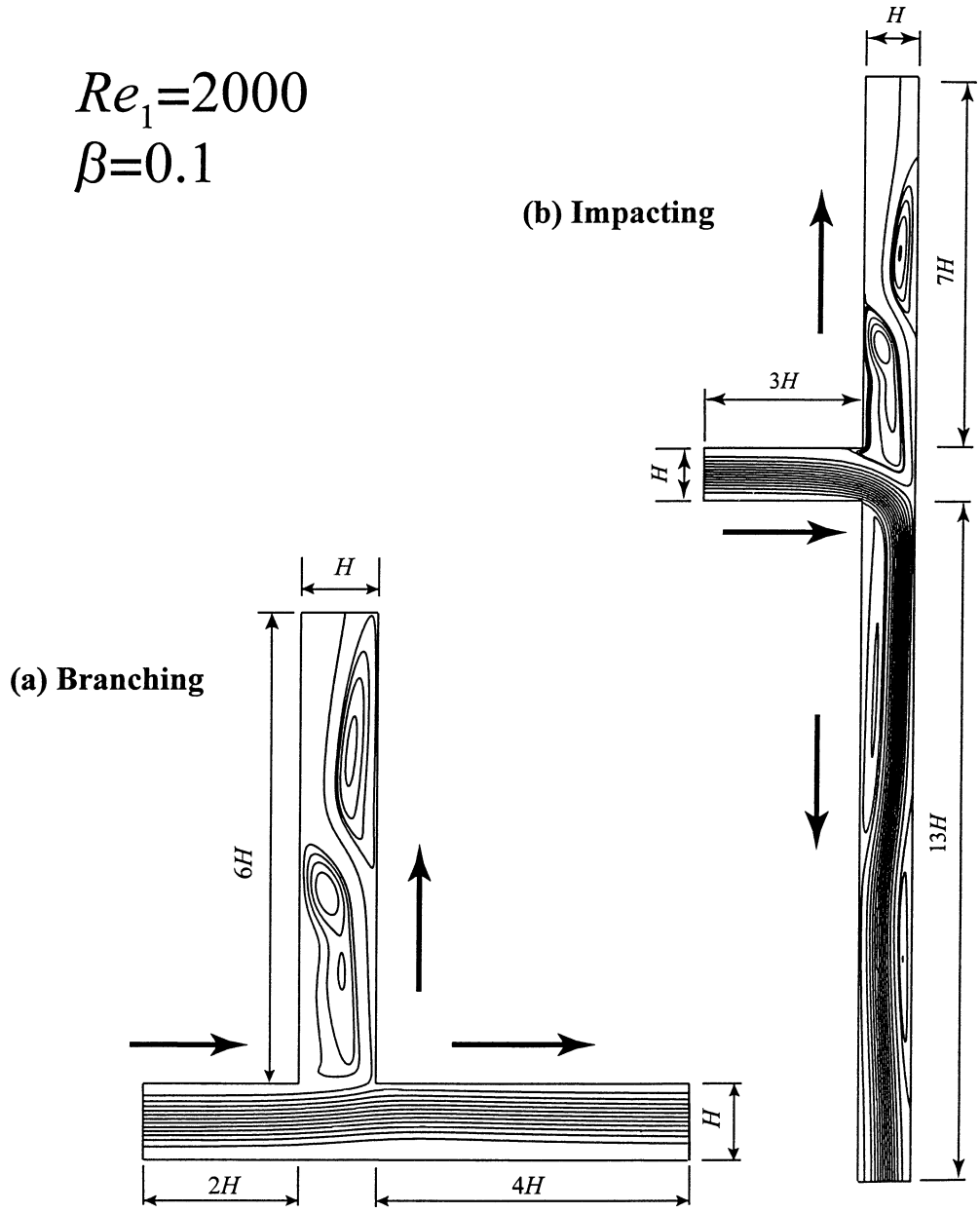

Fig. 9. Streamlines for $Re_1 = 2000$ and $\beta = 0.1$.

results of impacting tees is expected due to geometrical symmetry whereby, for example, a 30/70 mass split is just a mirror image of a 70/30 split. For the case of branching junctions, Fig. 14 shows that the value of E^* increases continuously with β. At low values of β, E^* for the branching junction is negative. This observation was also noted in the experimental study by McNown [9], who attributed the systematic occurrence of negative energy losses at low β to the fact that the kinetic energy terms in Eq. (9) were calculated using the average velocities rather than the velocity profiles. From Fig. 14, it may be concluded that the branching junction requires less pumping power up to $\beta \cong 0.4$, while the impacting junction requires less pumping power for $\beta \geqslant 0.4$.

4.5. Excess heat transfer

Another important parameter that can be used in evaluating the performance of the junction is the excess heat transfer Q_e defined as,

$$Q_e = Q - Q_{fd} \tag{11}$$

where Q is the total rate of heat transfer from all sides of the junction, and Q_{fd} is the total rate of heat transfer assuming fully-developed flow in all sides of the junction. Thus, Q_e reflects the effect of the junction on the rate of heat transfer. The value of Q_{fd} was calculated assuming fully developed conditions over the lengths L_1, L_{21}, and L_{31} (see Fig. 1) with mass flow rates $\dot{m}'_{in}$, $(1-\beta)\dot{m}'_{in}$, and $\beta\dot{m}'_{in}$ in sides

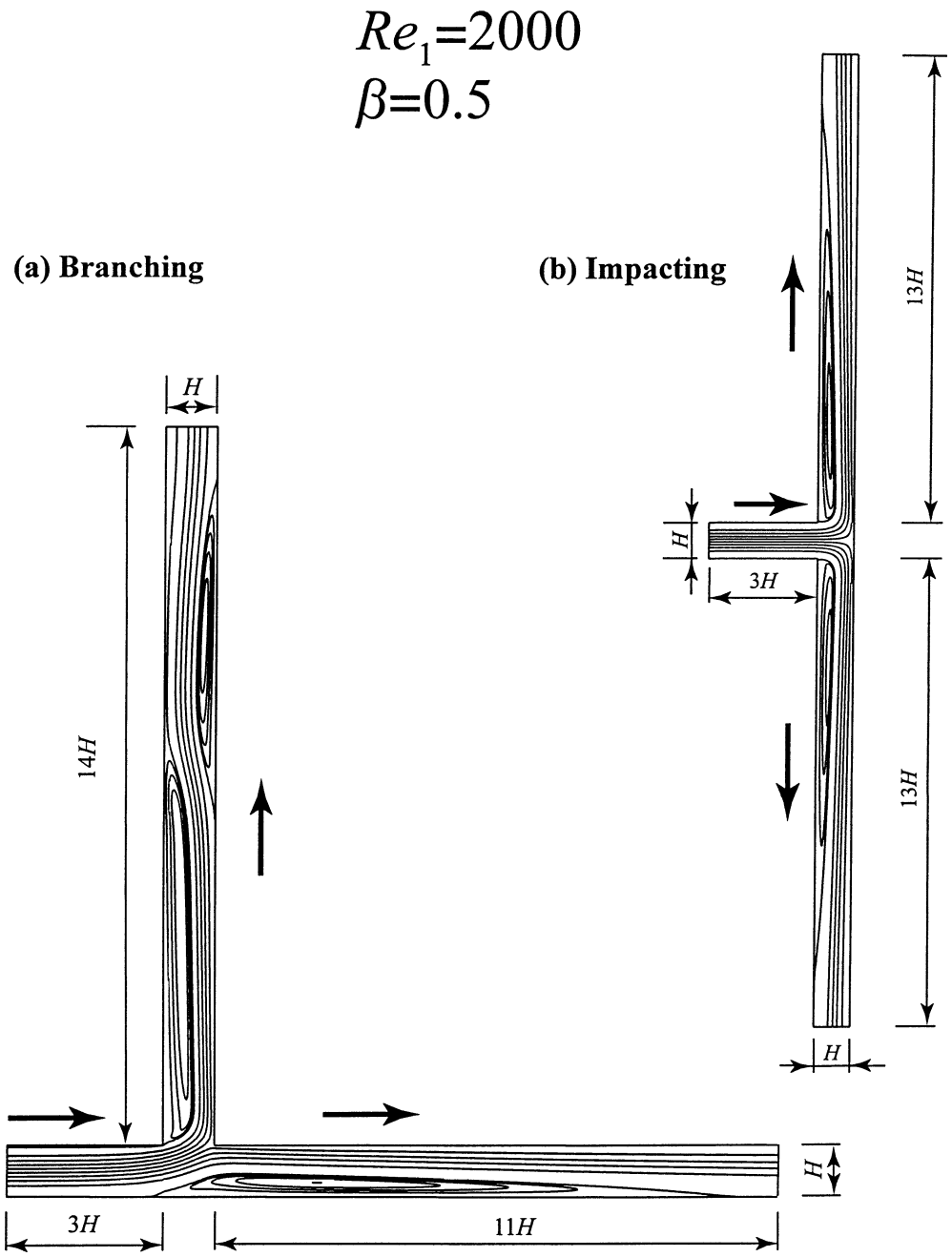

Fig. 10. Streamlines for $Re_1 = 2000$ and $\beta = 0.5$.

1, 2, and 3 of the junction. Under these conditions, Nusselt number has a value of 7.5407 [10]. The value of Q was calculated by integrating q_w over the whole surface area of the heat-transfer sections of the junction.

Fig. 15 shows the variation of Q_e^* $(= Q_e/[k(L_1^* + L_{21}^* + L_{31}^*)(T_w - T_{in})])$ with β for $Re_1 = 1000$ and 2000. It can be seen that Q_e^* is positive over the whole range of β except for the branching junction with $\beta \cong 0.1$. The fact that Q_e^* is positive indicates that the junction enhances the rate of heat transfer over fully developed conditions. The magnitude of this enhancement increases as Re_1 increases. The impacting junction produced the expected symmetrical behaviour with a maximum at $\beta = 0.5$ (the minor dip in the computed value at $\beta = 0.5$ and $Re_1 = 1000$ is not attributed to physical reasons). Finally, Fig. 15 shows that the impacting junction has higher values for Q_e^* in the range $0.1 \leqslant \beta < 0.4$ while the opposite is true in the range $0.4 < \beta \leqslant 0.9$.

The results in Figs. 14 and 15 do not give a clear win for either junction in the sense that when one junction gives a higher Q_e^*, it also requires a higher E^*. Therefore, the excess heat transfer per unit pumping power, Q_e^*/E^*, was calculated and the results are shown in Fig. 16. These results show that the branching junction has higher values of Q_e^*/E^* in the range $0.1 \leqslant \beta < 0.4$. In the range $0.4 \leqslant \beta <$

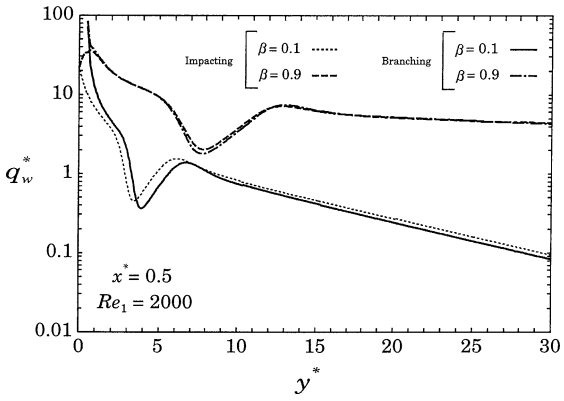

Fig. 11. Wall heat flux in outlet-3, $x^* = 0.5$.

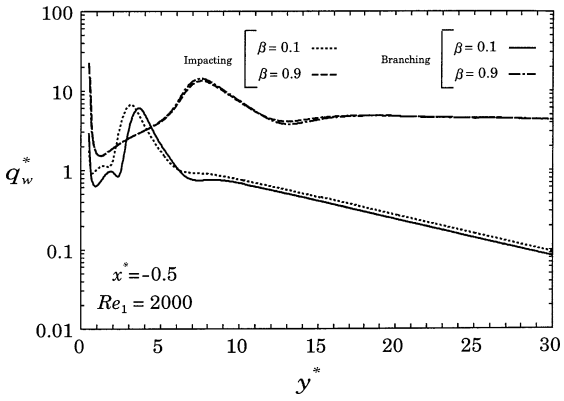

Fig. 12. Wall heat flux in outlet-3, $x^* = -0.5$.

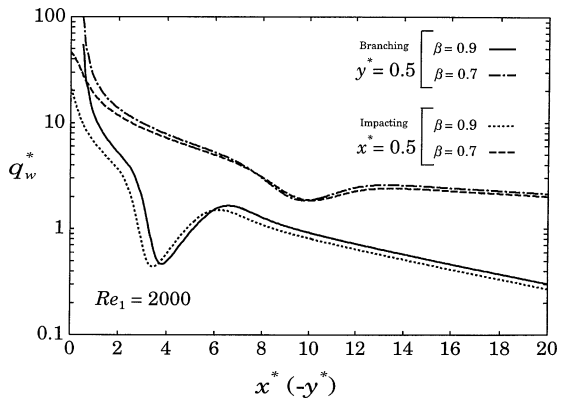

Fig. 13. Wall heat flux along one wall in outlet-2.

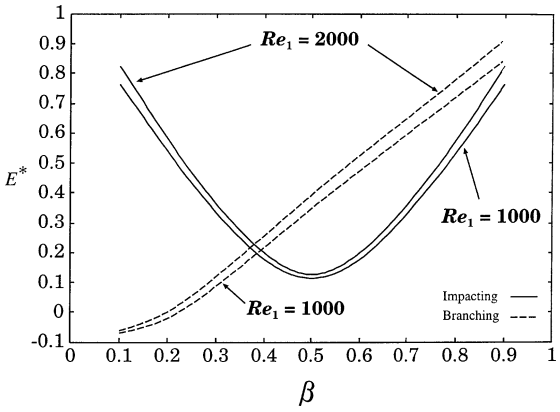

Fig. 14. Pumping power for both configurations.

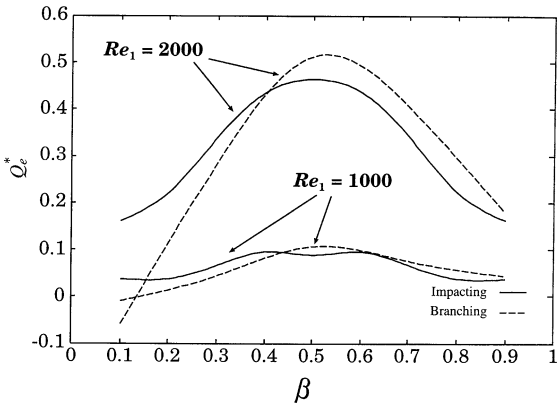

Fig. 15. Excess heat transfer for both configurations.

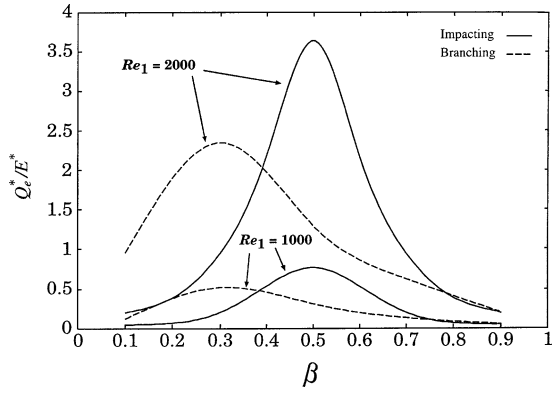

Fig. 16. Excess heat transfer per unit pumping power.

0.78, the impacting junction has higher values of Q_e^*/E^*, while for $\beta > 0.78$, the two junctions perform almost equally. These observations are valid for both values of Re_1 used in Fig. 16.

5. Conclusions

The following conclusions can be drawn from the present results:

(1) The two junctions have similar distributions for τ_w^* and q_w^* at $\beta = 0.1$ and 0.9. These similarities disappear at other mass splits.
(2) The branching junction requires less pumping power up to $\beta \cong 0.4$, while the impacting junction requires less pumping power for $\beta > 0.4$.
(3) The impacting junction provides better heat transfer up to $\beta = 0.4$, while the branching junction produces better heat transfer for $\beta > 0.4$.
(4) On the basis of excess heat per unit pumping power, the branching junction is superior up to $\beta \cong 0.4$.

Acknowledgements

The financial assistance provided by the Natural Sciences and Engineering Research Council of Canada is gratefully acknowledged.

References

[1] D. Liepsch, S. Moravec, A.K. Rastogi, N.S. Vlachos, Measurement and calculation of laminar flow in a ninety degree bifurcation, J. Biomech. 15 (1982) 473–485.
[2] J.M. Khodadadi, T. Nguyen, N.S. Vlachos, Laminar forced convective heat transfer in a two-dimensional 90° bifurcation, Numer. Heat Transfer 9 (1986) 677–695.
[3] T.G. Travers, W.M. Worek, Laminar fluid flow in a planar 90° bifurcation with and without a protruding branching duct, J. Fluids Engrg. 118 (1996) 81–84.
[4] A.M.F. El-Shaboury, H.M. Soliman, S.J. Ormiston, Laminar forced convection in two-dimensional equal-sided and reduced branching ducts, Numer. Heat Transfer 42 (2002) 487–512.
[5] D.K. Kreid, C.-J. Chung, C.T. Crowe, Measurement of the flow of water in a "T" junction by the LDV technique, J. Appl. Mech. 42 (1975) 498–499.
[6] J.S. Bramley, D. Sloan, Numerical solution for two-dimensional flow in a Branching channel using boundary-fitted coordinates, Comput. Fluids 15 (1987) 297–311.
[7] A.M.F. El-Shaboury, H.M. Soliman, S.J. Ormiston, Laminar forced convection in two-dimensional impacting tee junctions, Heat Mass Transfer, to appear.
[8] S.V. Patankar, Numerical Heat Transfer and Fluid Flow, Hemisphere, New York, 1980.
[9] J.S. McNown, Mechanics of manifold flow, ASCE Trans. 118 (1953) 1103–1142.
[10] R.K. Shah, A.L. London, Laminar Flow Forced Convection in Ducts, Academic Press, New York, 1978.